

Chapter 2

CAVITY RINGDOWN SPECTROSCOPY AND THE APPARATUS

2.1 Introduction to cavity ringdown spectroscopy

Detection of trace species in the gas phase is of interest to many scientific communities, including analytical and spectroscopic chemists. Applications range widely, from quantification of intermediates in the atmosphere to medical diagnosis to detection of dangerous explosives for national security.¹⁻⁸ A variety of methods have been developed to study radicals, including photoacoustic spectroscopy,⁹⁻¹¹ laser-induced fluorescence (LIF),^{12,13} and photoionization experiments.^{14,15} We focus on optical cavity techniques in this chapter.

Traditional absorption spectroscopic experiments consist of a sample cell, laser source, and detector. The Beer-Lambert Law states that:

$$I = I_0 e^{-\sigma NL} \quad (2.1 \text{ a})$$

where I = the intensity of light transmitted through the sample cell, I_0 = the intensity of the incident light, σ = the absorption cross section of the sample, N = the concentration of the species, and L = the pathlength of the absorbing sample. If the absorption cross section for a sample is known, the concentration of the species can be quantified. Difficulties arise when the cross section is small. The sensitivity of the technique could be vastly increased if the pathlength (L) is increased.

The method is also vulnerable to fluctuations in the laser intensity. If the cross section is small, the Beer-Lambert Law can be approximated as:

$$I = I_0 e^{-\sigma NL} \sim I_0(1 - \sigma NL) \quad (2.1 \text{ b})$$

With simple algebra, the equation is rewritten as:

$$\sigma NL = \frac{\Delta I}{I_0} \quad (2.1 \text{ c})$$

If ΔI is a small quantity, noise from laser fluctuations masks any measured absorption signal. The ultrasensitive optical cavity technique, cavity ringdown spectroscopy (CRDS), addresses both pathlength and laser power issues directly.

CRDS has been reviewed in the literature.^{6,7,16-19} We give a brief history and outline of the technique here. CRDS was developed in the early 1980s during experiments to measure the reflectivity of mirrors. These methods were quickly adapted to spectroscopic experiments.¹⁸ Two highly reflective mirrors ($R > 99.99\%$) are placed at the end of a sample cell (L) to form an optical cavity. This arrangement immediately addresses the issue of pathlength, as the sample cell of a few centimeters becomes equivalent to a pathlength of several kilometers. The overall sensitivity of the system is increased by 10^3 - 10^4 orders of magnitude.

A pulsed CRDS experiment illustrates the insensitivity of CRDS to fluctuations in the laser power (Fig. 2.1). A laser pulse with coherence less than L is injected into the empty cavity. When the pulse hits the surface of the mirror before the detector, $>99.99\%$ of the light is reflected back toward the first mirror. Some light ($T = 1 - R$) however is

transmitted to the detector. The pulse travels to the first mirror and loses intensity from transmission and mirror diffraction losses before it is reflected back to the other mirror. The transmitted light to the detector is less than the previous measurement. This process repeats until the detector can no longer measure the low intensity of the pulse. The pattern of the collected signal is a "ringdown."

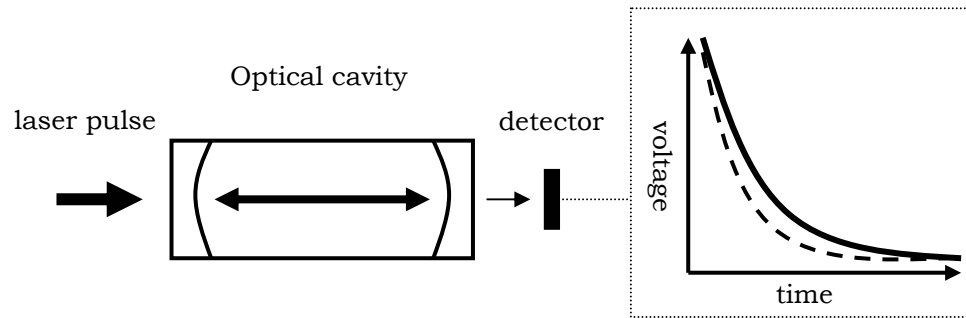


Figure 2.1. Schematic of a laser pulse injected into an optical cavity (L) for a pulsed CRDS experiment. The detector records signal from an empty cavity (bold line) and an absorber cavity (dashed line). The decay is much faster with the absorber cavity. By comparing the rates of decay, the absorption coefficient for the absorber can be extracted.

The losses in the empty cavity are described mathematically as:

$$\begin{aligned} \text{total loss} &= \frac{\# \text{ reflections}}{\text{trip}} \times \frac{\text{loss from transmission}}{\text{reflection}} \times \# \text{ trips} \\ &= 2 \times (1-R) \times \frac{tc}{2L} \end{aligned} \quad (2.2)$$

Following Beer-Lambert's law, we write for the empty cavity

$$I(t) = I_0 e^{-\frac{tc}{L}(1-R)} \quad (2.3)$$

and define a time constant or ringdown time τ_{vac} :

$$\tau_{vac} = \frac{L}{c(1-R)} \quad (2.4)$$

If an absorbing species is added to the cavity, then the total loss includes contribution from the sample absorbance:

$$\begin{aligned} \text{total loss} &= \frac{\# \text{ reflections}}{\text{trip}} \times \frac{\text{loss from transmission + absorbance}}{\text{reflection}} \times \# \text{ trips} \\ &= 2 \times [(1-R) + \sigma NL'] \times \frac{tc}{2L} \end{aligned} \quad (2.5)$$

where L' = the absorbance pathlength, which does not necessarily have to equal the pathlength of the optical cavity (L), e.g., the distance between the two reflective mirrors.

We then write for the absorbance cavity:

$$I(t) = I_0 e^{-\{(1-R) + \sigma NL'\} \frac{tc}{L}} \quad (2.6)$$

and ringdown time τ_{abs} :

$$\tau_{abs} = \frac{L}{c\{(1-R) + \sigma NL'\}} \quad (2.7)$$

The difference between the inverse of the absorber and vacuum ringdown times is directly related to the absorption coefficient a of the sample:

$$\alpha = \sigma N = \frac{L}{cL'} \left(\frac{1}{\tau_{abs}} - \frac{1}{\tau_{vac}} \right) \quad (2.8 \text{ a})$$

By comparing the rates of decay of a cavity with and without an absorber, the absorption coefficient of the sample can be measured. CRDS therefore does not suffer from fluctuations in the laser power, as the measurements are independent of intensity.

Current research on CRDS is focused on increasing the quality or Q -factor of the cavity. The Q -factor refers to the ratio of energy stored in the cavity versus the energy that is lost. Many groups have focused on coupling the laser to the modes of the cavity for efficient energy transfer. The sensitivities of CRDS and its variants have been reported to be on the order of 10^{-6} to 10^{-14} per pass.¹⁹⁻³⁴ The sensitivity of our pulsed CRDS apparatus is on the order of 10^{-6} to 10^{-8} per pass. Details on the calculation of our sensitivity are in Appendix 2.1.

The absorption coefficient is wavelength dependent. In expression 2.7 for the ringdown constant, both the reflectivity of the mirrors (R) and the absorption cross section of the sample (σ) is wavelength dependent. For spectroscopic experiments, both absorbance and vacuum (background) ringdowns must be collected at each spectral wavelength of interest. There are also other experimental factors to be considered for spectroscopic studies.

Lasers in spectroscopic measurements should be chosen such that their line widths are narrower than the width of the absorption of interest (Fig. 2.2). If a laser interacts with multiple absorption lines, the resulting signal has multi-exponential components. While absorption coefficients can be extracted,^{35,36} the analysis is more involved. The absorption cross section of the sample of interest also cannot be too large. Otherwise, the signal decays so rapidly that the detector cannot collect an adequate number of data points for exponential fit of the decay. Zalicki and Zare

calculated that the absorbance has to be less than $0.1(1-R)$ for accurate quantification.³⁵ Thus, CRDS is ideal for spectroscopic studies of trace gas species with relatively small absorption cross sections.

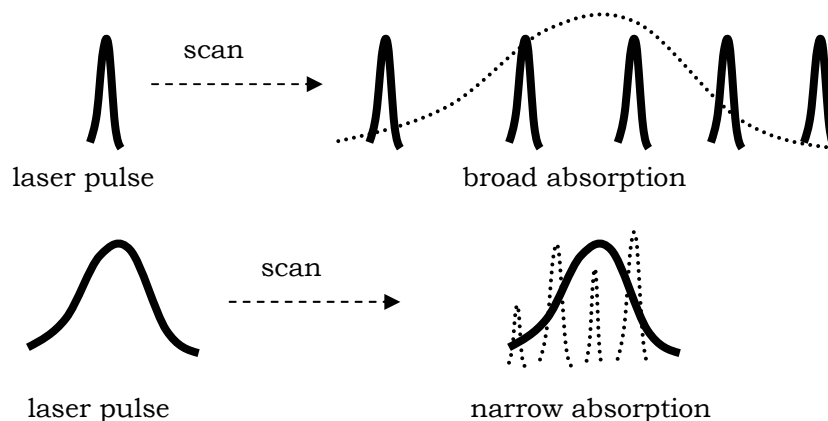


Figure 2.2. Illustrations of a laser (bold line) scanning over broad and narrow absorption lines (dotted lines). When the line width of the laser pulse is wider than the absorption lines, problems occur with the analysis, as multiple absorption lines interact with the laser, each with a different exponential decay constant.

For a 50-cm cell and mirrors $R = 0.9999$, the ringdown constant for an empty cavity is $16.7 \mu\text{s}$. If we generate 10^{14} radicals with cross sections $\sigma = 10^{-20} \text{ cm}^2$, the ringdown constant becomes $11.1 \mu\text{s}$. Thus, detection and kinetic measurements can be conducted on the microsecond timescale. We utilize both the sensitivity and fast time response of CRDS to probe trace atmospheric radicals in the near-infrared (NIR) region. We discuss in the next section the advantages of NIR detection and how we generate NIR light in our laboratory.

2.2 The Raman cell as a near-infrared source

While many tunable sources in the visible region are commercially available, there have historically been fewer options in the IR and even fewer options in the NIR regions. One of the main spectroscopic advantages of conducting experiments in the NIR region is less spectral interference. NIR transitions include vibrational overtones and low-lying

electronic transitions of radicals. The strengths of these transitions are orders of magnitude weaker than the line strengths in the visible region. Absorption by background species such as water is therefore significantly reduced. There is a trade-off as the radical of interest also has weaker absorption cross sections in the NIR region; however a sensitive technique such as CRDS can overcome these problems. The NIR has provided a new spectral window for many molecular species.³⁷⁻⁴²

Research on new IR sources has exploded in the past two decades. Advances include development of quantum cascade lasers, laser diodes, fiber optics, supercontinuum sources, and difference frequency generation in various crystals.⁴³⁻⁵⁰ The expense and simplicity of the sources vary widely. For laboratories that already utilize tunable visible sources, one simple and economic method to generate tunable NIR light is addition of a Raman cell to the apparatus. The underlying physics is discussed here, along with details of the Raman cell.

The Raman cell consists of a 2-m long metal cell with two silver-coated mirrors at each end. The mirrors have holes in their centers to allow passage of light in and out of the cell. The entrance port of the Raman cell includes an additional "pick-off" mirror attached to the mirror mount. The silver mirrors and pick-off mirror can be aligned in a multipass configuration. We generally operate in a 3-pass configuration, with 200 psi hydrogen in the Raman cell. Specific alignment procedures, along with photos of the cell, can be found in Appendix 2.2. Blueprints of the Raman cell have previously been published in a senior member's thesis.⁵¹

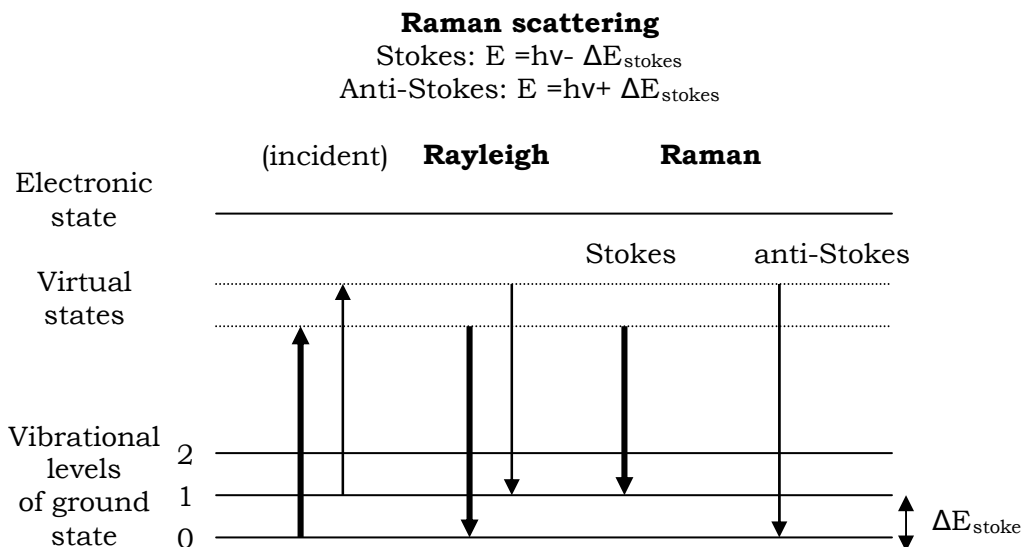


Figure 2.3. Diagram of the Rayleigh and Raman scattering upon interaction of the hydrogen molecules with incident light in the Raman cell. The majority of the light is Rayleigh scattered. Some light however is Raman-shifted to longer (Stokes shift) and shorter (anti-Stokes shift) wavelengths.

A diagram of the interaction between the hydrogen molecules and incident light is shown in Fig. 2.3. At room temperature, the majority of the hydrogen molecules occupy the ground electronic state. When light enters the cell, the molecules are excited to the virtual states. The virtual states are not electronic states; thus, these are not electronic transitions. Most of the hydrogen molecules relax back to the ground state, emitting photons of the same wavelength. This is Rayleigh scattering.

Some molecules, however, relax to the excited vibrational states rather than the ground state of hydrogen and emit photons of longer wavelengths (lower energy). This is Raman scattering, with the shift in the photon energy called the Stokes shift. The most intense band results from the first order Stokes shift, in which hydrogen molecules relax to the first vibrational state. The second most intense band results from

second order Stokes shift, in which hydrogen molecules relax to the second vibrational state.

At room temperature, there are some hydrogen molecules that already occupy vibrational levels of the ground state. Upon interaction with light, the same scattering phenomena occur. Some of the excited hydrogen molecules can relax to the ground state and emit photons of shorter wavelengths (higher energy). This shift in energy is called anti-Stokes shift. Due to Boltzmann weighting, the intensity of the anti-Stokes-bands is less than the Stokes bands.

The value of the Stokes shift is species dependent, as it relates to the vibrational level of the species. The Stokes shifts for several gases have been reported in the literature, including methane (2916 cm^{-1}) and hydrogen (4155 cm^{-1}).^{52,53} We use hydrogen in our Raman cell. In a typical experiment, the incident light is in the visible region (e.g., $\lambda = 640\text{ nm}$ at 10 mJ/pulse). The first and second order Stokes outputs ($<1\text{ mJ/pulse}$) are then 872 nm (11470 cm^{-1}) and 1367 nm (7315 cm^{-1}), respectively. As we use a tunable dye laser to generate visible light, the incident light can easily be tuned to generate tunable NIR light for the CRDS experiments.

2.3 The pulsed CRDS apparatus

We use pulsed CRDS to study vibronic transitions of atmospheric species in the NIR region. A diagram of the apparatus is shown in Fig. 2.4. A Nd:YAG laser (Continuum NY61, 532 nm at $100\text{-}150\text{ mJ/pulse}$) is fired at $5/20\text{ Hz}$ to pump a tunable dye laser (Continuum TDL51, $\Gamma = 0.15\text{ cm}^{-1}$), generating $10\text{-}15\text{ mJ/pulse}$ of visible light. Before entering the Raman cell ($P_{H_2} = 200\text{ psi}$), the beam is propagated by various optics to reduce hot spots and obtain a Gaussian or TM00 mode beam profile. Telescope lens

are used to adjust the beam diameter such that the laser pulse does not harm the silver mirrors of the Raman cell. The beam however is focused inside the Raman cell for optimum NIR conversion.

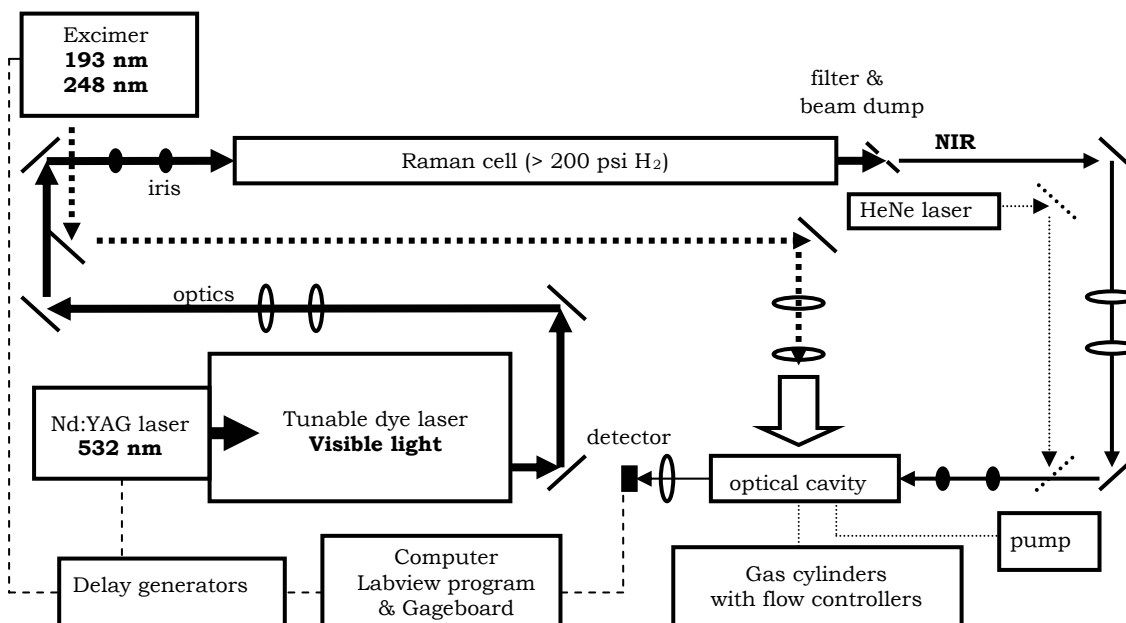


Figure 2.4. Schematics of our pulsed CRDS apparatus. The HeNe laser is used for alignment of the optical cavity. Each of the components are discussed in the Chapter 2 appendix. The sensitivity of the apparatus ranges from $\alpha = 10^{-6}$ to 10^{-8} per pass, depending on the CRD mirror and ringdown cell utilized in the optical cavity.

Upon exit of the Raman cell, a silicon filter is used to isolate the NIR light of interest (< 1 mJ/pulse). The NIR light is directed toward the optical cavity, with another set of telescope lens to re-focus the beam. After the laser pulse enters the optical cavity, NIR signal is focused with a 10-mm focal lens and collected by a 1-mm diameter InGaAs photodiode with a built-in transimpedance amplifier (Thorlabs PDA 400). Each decay is recorded by a transient digitizer computer board (Gage Compuscope 14100), operating at 20 MHz sampling rate. Five to twenty waveforms are collected before being averaged and fit with an exponential curve in our Labview data collection and analysis program. An overview of the

Labview program is provided in Appendix 2.3.1. The sensitivity of our apparatus ranges from 10^{-6} to 10^{-8} per pass.

The optical cavity is shown in Fig. 2.5. The optical cavity has been designed to simply alignment while maximizing flexibility. Two metal flanges with CRD mirrors mounts (Newport) are attached to Pyrex couplers that connect directly to the ringdown cell. Windows on the flanges allow NIR light to enter the cell. They also maintain the pressure of the cell. The flanges include gas ports such that helium/nitrogen purge gases can be flowed during the experiments to protect the CRD mirrors. Blueprints of the flanges have been previously published.⁵¹

We use a variety of Pyrex and stainless steel ringdown cells for our experiments. The choice of ringdown cell depends highly on the nature of the experiment. Most ringdown cells have multiple ports for chemical gas input and pressure readout. As we conduct most experiments under flow conditions, we also connect our ringdown cell to the mechanical vacuum pump. To minimize wall-reactions, many of the cells are coated with Fluoropel. There are various types of Fluoropel. Some are UV-sensitive; others do not adhere to stainless steel. The appropriate Fluoropel sample should be used to coat the ringdown cell for each experiment.

The volumes of the ringdown cells can also largely vary. While it is advantageous to have larger concentrations of radicals for CRDS detection, the mechanical pump has a limited pumping rate. For large volumes, the flow rates of the gases are reduced, increasing the residence time of the reacting species inside the cell. Some radicals have long lifetimes (\sim ms) and can be studied under long residence time conditions. In other cases, especially for the kinetic experiments, a small volume cell

must be used. Diagrams of the ringdown cells and a list of our CRD mirrors are available in Appendix 2.3.2. The alignment of the optical cavity is also discussed in the appendix.

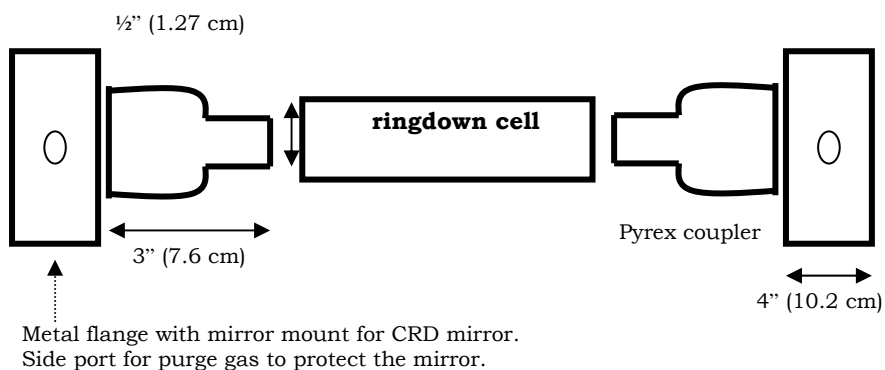


Figure 2.5. Diagram of the CRD optical cavity used in our laboratory. The ringdown cell can be easily decoupled from the apparatus such that we can switch in and out the desired cell. The metal flanges holding the CRD mirrors can also be removed without disturbing the ringdown cell such that we can clean or switch the CRD mirrors between experiments.

We conduct experiments over a large wavelength region of interest. Due to the simplicity of the Raman cell, scanning across a large wavelength region mostly involves changing the dyes of the dye laser and the CRD mirrors of the optical cavity. For each dye change, the dye laser is realigned and optimized for power. The position of the dye laser wavelength is also recalibrated. We use a combination of optogalvanic spectroscopy and CRDS for calibration. Details are available in Appendix 2.3.3. The recipes for the various laser dyes covering the 580-670 nm region are also provided in the appendix.

In general, the Nd:YAG and dye lasers used in the apparatus are very durable and, with basic maintenance, can be used for a long time in the laboratory. We provide notes on the general maintenance of the lasers in Appendix 2.3.4. We also utilize a third laser for many of the kinetic

experiments, the fluorine excimer laser. The fluorine excimer laser (Lambda Physik LPF 220, 193/248 nm: 60-150 mJ/pulse) generates high energy UV pulses to initiate radical formation. We control the timing between the firing of the fluorine excimer and Nd:YAG (probe) lasers such that time-resolved measurements can be made. The timing conditions are discussed in Appendix 2.3.5.

The shape and size of the excimer beam are controlled by two optical lens, an UV fused silica plano-convex cylindrical lens (Thorlabs F-500mm) and an UV plano-concave lens (Edmund Optics 50.8 mm x 100 FL). The excimer beam is focused 0.5~1-cm wide and stretched to match the dimensions of the quartz window of the ringdown cell. Measurements of the excimer power are made at both the exit of the laser and directly before the ringdown cell. This is especially critical in the case of 193-nm light, as absorption by oxygen greatly decreases the power of light over a long distance. We use a beam blocker, in conjunction with a power detector, to check that the excimer beam profile is uniform.

Photolytic chemical systems are also used to characterize the excimer laser source. We align the UV lenses to maximize radical production. If the reactant concentrations and the photolysis rates are known, we can quantify the amount of radical formation and directly calculate the energy of the excimer pulse inside the ringdown cell. Specific details are given in Chapter 5. Discussion on the chemical methods and modeled kinetics of nitrate and substituted peroxy radicals are reserved until their respective chapters.

2.4 Summary

In this chapter, we discussed the chemical physics behind CRDS and provided details of the pulsed CRDS apparatus used in our experiments. The advantages of spectroscopic studies in the NIR region were also outlined. The appendix for Chapter 2 contains a detailed account of the lasers and computer programs used in our laboratory. Appendix 2.4 is particularly recommended for persons interested in working in the laboratory, as it reviews many lab safety issues.

As we better understand the CRDS apparatus, we discuss in the next chapters the different chemical systems and radicals probed by the apparatus. In Chapter 1, we showed that the understanding of the Earth's atmosphere involves elucidation of both the chemical physics and kinetics of a radical. We begin in the next chapter with a chemical physics perspective. The problem however maintains a firm root in atmospheric chemistry, as we focus on analysis of the most important nighttime oxidant in the troposphere, the nitrate radical.

2.5 References

- (1) Fiddler, M. N.; Begashaw, I.; Mickens, M. A.; Collingwood, M. S.; Assefa, Z.; Bililign, S. *Sensors* **2009**, *9*, 10447.
- (2) Nakaema, W. M.; Hao, Z. Q.; Rohwetter, P.; Woste, L.; Stelmaszczyk, K. *Sensors* **2011**, *11*, 1620.
- (3) Wang, C. J.; Sahay, P. *Sensors* **2009**, *9*, 8230.
- (4) Senesac, L.; Thundat, T. G. *Mater. Today* **2008**, *11*, 28.
- (5) Wallin, S.; Pettersson, A.; Ostmark, H.; Hobro, A. *Anal. Bioanal. Chem.* **2009**, *395*, 259.
- (6) Friedrichs, G. *Zeitschrift Fur Physikalische Chemie-International Journal of Research in Physical Chemistry & Chemical Physics* **2008**, *222*, 31.
- (7) Wheeler, M. D.; Newman, S. M.; Orr-Ewing, A. J.; Ashfold, M.N. R. *Journal of the Chemical Society-Faraday Transactions* **1998**, *94*, 337.
- (8) Ball, S. M.; Jones, R. L. *Chemical Reviews* **2003**, *103*, 5239.
- (9) Zoltan, B.; Andrea, P.; Gabor, S. *Applied Spectroscopy Reviews* **2011**, *46*, 1.
- (10) Foster, N. S.; Autrey, S. T.; Amonette, J. E.; Small, J. R.; Small, E. W. *American Laboratory* **1999**, *31*, 96S.
- (11) Bertrand, L. G. *Journal of the Optical Society of America a-Optics Image Science and Vision* **1985**, *2*, P6.
- (12) Daily, J. W. *Progress in Energy and Combustion Science* **1997**, *23*, 133.
- (13) Kohsehoinghaus, K. *Progress in Energy and Combustion Science* **1994**, *20*, 203.
- (14) Zimmermann, R.; Welthagen, W.; Groger, T. *Journal of Chromatography A* **2008**, *1184*, 296.
- (15) Ledingham, K. W. D.; Singhal, R. P. *International Journal of Mass Spectrometry and Ion Processes* **1997**, *163*, 149.
- (16) Brown, S. S.; Stark, H.; Ravishankara, A. R. *Applied Physics B-Lasers and Optics* **2002**, *75*, 173.
- (17) *Cavity Ringdown Spectroscopy: An Ultratrace-Absorption Measurement Technique*; Busch, K. W.; Busch, M. A., Eds.; Oxford University Press, 1999.
- (18) Scherer, J. J.; Paul, J. B.; Okeefe, A.; Saykally, R. J. *Chemical Reviews* **1997**, *97*, 25.
- (19) Berden, G.; Peeters, R.; Meijer, G. *International Reviews in Physical Chemistry* **2000**, *19*, 565.
- (20) Foltynowicz, A.; Ma, W. G.; Axner, O. *Optics Express* **2008**, *16*, 14689.

- (21) Engel, G. S.; Drisdell, W. S.; Keutsch, F. N.; Moyer, E. J.; Anderson, J. G. *Applied Optics* **2006**, *45*, 9221.
- (22) O'Keefe, A.; Scherer, J. J.; Paul, J. B. *Chemical Physics Letters* **1999**, *307*, 343.
- (23) Berden, G.; Peeters, R.; Meijer, G. *Chemical Physics Letters* **1999**, *307*, 131.
- (24) Peeters, R.; Berden, G.; Meijer, G. *American Laboratory* **2001**, *33*, 60.
- (25) Foltynowicz, A.; Schmidt, F. M.; Ma, W.; Axner, O. *Applied Physics B - Lasers and Optics* **2008**, *92*, 313.
- (26) Schmidt, F. M.; Foltynowicz, A.; Ma, W. G.; Lock, T.; Axner, O. *Optics Express* **2007**, *15*, 10822.
- (27) van Leeuwen, N. J.; Wilson, A. C. *Journal of the Optical Society of America B-Optical Physics* **2004**, *21*, 1713.
- (28) Hall, J. L.; Ye, J.; Diddams, S. A.; Ma, L. S.; Cundiff, S. T.; Jones, D. J. *Ieee Journal of Quantum Electronics* **2001**, *37*, 1482.
- (29) Ye, J.; Hall, J. L. *Physical Review A* **2000**, *61*.
- (30) Ye, J.; Hall, J. L.; Diddams, S. A. *Optics Letters* **2000**, *25*, 1675.
- (31) Yoon, T. H.; Ye, J.; Hall, J. L.; Chartier, J. M. *Applied Physics B-Lasers and Optics* **2001**, *72*, 221.
- (32) Ma, L. S.; Ye, J.; Dube, P.; Hall, J. L. *Journal of the Optical Society of America B-Optical Physics* **1999**, *16*, 2255.
- (33) Havey, D. K.; Long, D. A.; Okumura, M.; Miller, C. E.; Hodges, J. T. *Chemical Physics Letters* **2009**, *483*, 49.
- (34) Long, D. A.; Havey, D. K.; Okumura, M.; Miller, C. E.; Hodges, J. T. *Physical Review A* **2010**, *81*.
- (35) Zalicki, P.; Zare, R. N. *Journal of Chemical Physics* **1995**, *102*, 2708.
- (36) Mollner, A., *Ph. D. Thesis*, California Institute of Technology, 2007.
- (37) Donaldson, D. J.; Tuck, A. F.; Vaida, V. *Chemical Reviews* **2003**, *103*, 4717.
- (38) Vaida, V. *Journal of Physical Chemistry A* **2009**, *113*, 5.
- (39) Sharp, E. N.; Rupper, P.; Miller, T. A. *Physical Chemistry Chemical Physics* **2008**, *10*, 3955.
- (40) Liu, Z. W.; Xu, Y.; Yang, X. F.; Zhu, A. M.; Zhao, G. L.; Wang, W. G. *Journal of Physics D - Applied Physics* **2008**, *41*.
- (41) Enami, S.; Yamanaka, T.; Hashimoto, S.; Kawasaki, M.; Aloisio, S.; Tachikawa, H. *Journal of Chemical Physics* **2006**, *125*.
- (42) Hirota, E.; Ishiwata, T.; Kawaguchi, K.; Fujitake, M.; Ohashi, N.; Tanaka, I. *Journal of Chemical Physics* **1997**, *107*, 2829.

- (43) Angel, S. M.; Carrabba, M.; Cooney, T. F. *Spectroc. Acta Pt. A-Molec. Biomolec. Spectr.* **1995**, 51, 1779.
- (44) Curl, R. F.; Capasso, F.; Gmachl, C.; Kosterev, A. A.; McManus, B.; Lewicki, R.; Pusharsky, M.; Wysocki, G.; Tittel, F. K. *Chemical Physics Letters* **2010**, 487, 1.
- (45) Fischer, C.; Sigrist, M. W. In *Solid-State Mid-Infrared Laser Sources*; Springer-Verlag Berlin: Berlin, 2003; Vol. 89, p 97.
- (46) Gmachl, C.; Capasso, F.; Sivco, D. L.; Cho, A. Y. *Reports on Progress in Physics* **2001**, 64, 1533.
- (47) Hugi, A.; Maulini, R.; Faist, J. *Semiconductor Science and Technology* **2010**, 25.
- (48) Richter, D.; Fried, A.; Weibring, P. *Laser & Photonics Reviews* **2009**, 3, 343.
- (49) van Helden, J. H.; Hancock, G.; Peverall, R.; Ritchie, G. A. D. *Journal of Physics D - Applied Physics* **2011**, 44.
- (50) Yin, S.; Ruffin, P.; Brantley, C.; Edwards, E.; Yang, C. E.; Luo, C. In *Photonic Fiber and Crystal Devices: Advances in Materials and Innovations in Device Applications Iv*; Yin, S., Guo, R., Eds. 2010; Vol. 7781.
- (51) Deev, A., California Institute of Technology, 2005.
- (52) Rabinowitz, P.; Perry, B. N.; Levinos, N. *IEEE Journal of Quantum Electronics* **1986**, 22, 797.
- (53) Aniolek, K. W.; Miller, D. L.; Cernansky, N. P.; Owens, K. G. *Applied Spectroscopy* **1997**, 51, 820.